The Bioscan AN INTERNATIONAL QUARTERLY JOURNAL OF LIFE SCIENCES 20(3): 57-67, 2025 www.thebioscan.com

Cardiospermum halicacabum derived MoO_3 nanoparticles for Fluorescence sensing, DNA binding and Cytotoxicity Studies

Sanniyasi Rajeswari[1,a], Seth Sheeba Thavamani[1]*

[1]Post Graduate and Research Department of Chemistry, V.O. Chidambaram College, Tuticorin–628008, Tamil Nadu, India, e-mail: sheeb.che@voccollege.ac.in, Tel: +91 461-2310175; Fax: +91 461-2310275, ORCID: 0000-0002-7577-6343

[a]Research Scholar, Reg. No: 19222232032008, Post Graduate and Research Department of Chemistry, V.O. Chidambaram College, Tuticorin–628008, (Affiliated to Manonmaniam Sundaranar University, Tirunelveli), Tamil Nadu, ORCID: 0009-0006-6332-2367

DOI: 10.63001/tbs.2025.v20.i03.pp57-67

KEYWORDS
biosynthesis, Cardiospermum halicacabum, cytotoxicity, DNA binding, MoO3 nanoparticles

Received on:

10-05-2025

Accepted on:

07-06-2025

Published on:

07-07-2025

ABSTRACT

MoO_3 nanoparticles were biosynthesised using *Cardiospermum halicacabum* leaf extract. Their structural and morphological properties were investigated through UV–visible DRS studies, photoluminescence, Fourier Transform Infra-Red spectroscopy, Energy-Dispersive X-ray analysis, X-Ray Diffraction, X-Ray Photoelectron Spectroscopy and High-Resolution Transmission Electron Microscopy. $O^{2-} \rightarrow Mo^{6+}$ transition was confirmed by the peak observed at 353nm in UV-Visible spectrum and the band gap was estimated as 2.48 eV. Mo-O-Mo bond was confirmed by the bands observed at 842 cm^{-1} and 475 cm^{-1} in FTIR spectroscopy. EDX spectra showed characteristic peaks of oxygen and molybdenum. XPS showed binding energies of 232.4 and 235.6 eV, which correspond to spin-orbit splitting of Mo $3d_{5/2}$ and Mo $3d_{3/2}$ respectively, which confirmed that Mo is present in +6 state. The particle size was determined to be 69 nm using XRD analysis. Effective fluorescence sensing of Pb^{2+} was observed with a detection limit 4.13×10^{-8} M. ct-DNA binding constant was calculated as 3.09 $(mg/mL)^{-1}$ and 2.32 $(mg/mL)^{-1}$ using UV-Vis and fluorescence studies respectively. Cytotoxicity studies using A549 Human Lung cancer cell line showed IC_{50} value of 249.5 µg/mL

INTRODUCTION

Nanomaterials having structural features between bulk materials and atoms find fascinating applications in diverse fields and their demand keeps increasing. Their unique optical, physical, and chemical properties have rooted applications as catalysts, chemical sensors, optoelectronics, bioimaging agents, and pharmaceutical products. Their biocompatibility finds utility in diagnosis, drug delivery and in pharmaceutical formulations [1,2]. In the last few decades, transition metal oxides have attracted the research community in great deal due to their diversified applications. Great consideration of nanomaterials has been paid to the fabrication of various kinds of nanometal oxides like TiO_2, ZnO, ZrO_2, CuO, MgO, etc., Among these metal oxide, MoO_3 nanoparticles are fascinating due to their low-cost, higher chemical stability, distinct, unique structural, optical, electrical, and mechanical properties. They are applied successfully in multiple applications of various fields, such as photocatalysis, light emitting diodes, therapies, gas sensing, and in many medical protocols [3].

Nanoparticles (NPs) are synthesized by several methods including coprecipitation, laser ablation, hydrothermal, sol-gel method, microwave-assisted technique, pyrolysis, and thermal decomposition. Conventional synthetic techniques are not eco-friendly and are expensive, which draws interest toward green synthesis. Green synthetic routes address these issues and grab interest due to their biocompatibility and renewability [4,5]. Green synthetic routes utilize phytochemical constituents such as phenols, flavonoids, tannins, alkaloids, and quinines as reducing, stabilizing, and capping agents. Thus, they find desired applications in medicine, agriculture, and environmental remediation. They exhibit enhanced reactivity due to organic capping moieties [1,6].

Metal ion recognition and sensing have become a fast-growing area of research due to their potential application in chemistry, biomedicine, and environmental studies. The toxicity and effect of trace heavy metals on human health and the environment have attracted considerable attention and concern in recent years. Lead toxicity leads to dysfunction of the kidney, reproductive system, and brain while chronic damages are caused to the Central Nervous System and Peripheral Nervous System. Lead also inhibits the synthesis of haemoglobin. Pregnant women with low calcium, iron or zinc levels are prone to the effects of lead accumulation [7]. In the environment, Pb^{2+} in any form cause harms to crops, soil, water, air, and other edible materials [8].

DNA serves as a memory storage for genetic information and is the main target molecule for a majority of antiviral and anticancer treatments. The interaction of drugs with DNA plays a crucial rule in development of medicinal compounds [9,10]. Recent studies in the fields of biology, chemistry, and clinical medicine have focused on the interaction between medicines and DNA. Anti-

bacterial, anti-tumour and antiviral drugs function effectively by binding to genomic DNA. Metal complexes owing to their superior antioxidant activity, cytotoxic activity and DNA binding ability interact with DNA and pave way for development of anticancer drugs, sequence-specific cleaving agents, and efficient chemotherapeutic agents for a variety of diseases. These interactions also offer pathways towards rational drug design [11]. Various binding methods are used to study the mode of drug–DNA interactions, such as thermal denaturation studies, KI quenching studies, foot printing assay, CD spectroscopy, FT-IR spectroscopy, isothermal titration calorimetry, atomic force microscopy, Cyclic Voltammetry, Nuclear Magnetic Resonance, molecular docking, UV–visible spectroscopy and fluorescence spectroscopy [12].

Lung cancer is the second most common disease leading to cancer-related mortality, taking lives of more people than colorectal, prostate, and breast cancers put together. Cytotoxicity evaluation of NPs shows that they can cross biological barriers and assemble in many organs, exhibiting harmful consequences such oxidative stress, DNA damage, cell death, and morphological alterations [1]. *Cardiospermum halicacabum* belongs to the family Sapindaceae commonly known as balloon vine. *C. halicacabum* is used as a green vegetable. The presence of saponins results in foam formation when agitated with water and hence, it is used as hair detergent and soap for laundry. Each part of the plant is beneficial and is used as food and used to treat stiffness of limbs, snake bite, and rheumatism. In Ayurveda and folk medicine, this plant is used to treat fever, lumbago, and earache. It is also used as stomachic, rubefacient, and diuretic. *Cardiospermum halicacabum* exhibits antioxidant, anti-viral, anti-ulcer activity, anti-diabetic, anti-convulsant, antipyretic, anxiolytic, anti-cancer, anti-bacterial, anti-arthritic, anti-fungal, antiparasitic, anti-diarrheal, adulticidal, anti-filarial, anti-malarial, anti-inflammatory and anti-sickling activities. This herb is useful to produce commercial drugs because of the existence of constituents such as beta-sitosterol along with D-glucosides, amino acids, oxalic acid, saponins, quebrachitol, oleic acid, eicosonic acid, erucic acid, octanoic acid, n-hexadecenoic acid, and triterpenoids. *Cardiospermum halicacabum* is used in unique systems of medication along with Homeopathy, Unani, and Ayurvedic medicine. The presence of several phytoconstituents such as flavonoids, tannins, and alkaloids have also been reported in phytochemical analysis [13].

This work focuses on (i) synthesis of MoO_3 NPs using *Cardiospermum halicacabum* leaf extract, (b) characterization of the prepared NPs using UV-Visible Diffuse Reflectance Spectroscopy (UV-Vis DRS), photoluminescence spectroscopy (PL), Fourier transform infra-red spectroscopy (FT-IR), energy-dispersive X-ray analysis (EDX), X-ray diffraction (XRD), X-ray photoelectron spectroscopy (XPS), and high-resolution transmission electron microscopy (HRTEM), and (iii) potential applications of NPs towards fluorescent sensing of Pb^{2+}, ct-DNA binding ability using absorbance and fluorescence spectra, and cytotoxic behaviour against A 549 (human lung cancer) cells.

2. Experimental Section

2.1. Materials and Methods

Ammonium molybdate tetrahydrate manufactured by Sisco Research Laboratories Pvt. Ltd. of assay 99.5% was used as the precursor for the preparation of nanoparticles. *Cardiospermum halicacabum* leaves were collected from Kattalankulam, Tamil Nadu, India. JASCO FP-8300 spectrofluorometer and V-650 spectrophotometer were employed to study the electronic and optical properties of the nanoparticles. The functional groups present in *Cardiospermum halicacabum* leaves extract, which contribute for the formation and stabilization of MoO_3 NPs were identified by recording FT-IR spectra using SHIMADZU, IRTRACER 100 in the range 400–4000 cm^{-1}. Crystallinity and phase morphology of green synthesized MoO_3 NPs were characterized by powder X-Ray Diffractometer (X' Pert Pro, PAnalytic). The elements present in the synthesized MoO_3NPs were analysed by EDAX using Bruker Nano, GmbH, D-12489 at an accelerating voltage of 30 kV. X-ray photoelectron spectroscopy (Physical Electronics, PHI Versaprobe III) was used to investigate the ionic valence of Mo and O. HR-TEM analysis using Jeol/JEM 2100 (200kV) was used to determine the size and shape of the nanoparticles. ct (calf–thymus) DNA employed for DNA binding studies was purchased from Bio Gen, Bangalore. Ethidium bromide used for fluorescence DNA binding studies (assay 95.0%) was purchased from Sigma-Aldrich. Human lung cancer cell line (A549) procured from National Centre for Cell Sciences (NCCS), Pune, India, was used for cytotoxicity studies.

2.2. Preparation of *Cardiospermum halicacabum* extract

20 g of *Cardiospermum halicacabum* leaves were mixed with 100 mL of double distilled water and warmed at 50 ºC for 30 min. The extract was cooled and filtered through Whatmann No.1 filter paper and stored in a refrigerator at 4 ºC and was used within a week for the synthesis process.

2.3. Green Synthesis of MoO_3 Nanoparticles (MoO_3 NPs)

20 mL of the prepared *Cardiospermum halicacabum* extract was added dropwise to 10 mL of 0.1 M aqueous solution of ammonium molybdate tetrahydrate and was subjected to magnetic stirring for 4 h. The resultant brown precipitate (due to adsorption of *Cardiospermum halicacabum* extract) was allowed to stand for 24 h and was centrifuged at 4000 rpm for 15 min, washed thoroughly with double distilled water and ethanol to ensure the elimination of soluble biocomponents and dried at 90 °C in an air oven. It was further finely powdered and calcined in a muffle furnace for 6 h at 600 °C, which resulted in green MoO_3 NPs.

2.4. Fluorescent Sensing of Pb^{2+}

MoO_3 NPs (10 mg) were dispersed in 10 mL of water and 0.2 mL of the dispersed NPs solution was mixed with 1.8 mL of 100 µM aqueous solution of Pb^{2+} to study the fluorescence behaviour. A series of aqueous solution of metal ions namely, Cd^{2+}, Zn^{2+}, V^{2+}, Nd^{3+}, Fe^{2+}, Fe^{3+}, Cu^{2+}, Sr^{2+}, La^{3+}, Pb^{2+}, Ni^{2+}, Co^{2+}, $Cr^{3+}$and Hg^{2+}ions were chosen for selectivity studies under identical conditions. As Pb^{2+} showed maximum enhancement in fluorescence intensity, the aqueous suspension of MoO_3 NPs was further explored towards fluorescent sensing of Pb^{2+}. To establish the prepared MoO_3 NPs as fluorescent sensors for Pb^{2+}, the dispersed solution of MoO_3 NPs was treated with 1.8 mL of $Pb^{2+}$of varying concentrations from 0.01 µM to 100 µM, allowed to stand for 2 min to facilitate interaction and photoluminescence was monitored. The limit of detection was calculated using Equation (1).

$$LOD = \frac{3Sb}{m} \text{ ---------- Eq.(1)}$$

where "Sb" and "*m*" denote the standard deviation of blank (*n* = 10) and the slope of the standard curve, respectively

2.5. DNA binding studies

The interaction between MoO_3 NPs and calf thymus DNA (ct-DNA) was examined using in vitro DNA binding studies using UV–Visible spectroscopy. A stock solution with 6 mg of ct-DNA in 10 mL of 0.1 M Tris-HCl buffer (pH 7.2) was prepared. 10 mg MoO_3 NPs were dispersed in 10 mL of buffer solution and subsequently added to the DNA solution, varying the concentration of MoO_3 NPs from 0.005 mg/mL to 0.050 mg/mL while maintaining a constant total volume of 2 mL. The resultant solution was sonicated for 20 min at room temperature. Keeping the volume of ct-DNA at 100 µL constant, the dosage of MoO_3 NPs was varied, adjusting the total volume to 2 mL by tris-HCl buffer, UV-Visible spectra were recorded to monitor the binding efficiency. The binding constant (K) was evaluated using Benesi-Hildebrand equation [equation (2)] [14].

$$\frac{1}{(A_{obs}-A_0)} = \frac{1}{(A_c-A_0)} + \frac{1}{K(A_c-A_0)[MoO_3\ NPs]} \text{ -------Eq.(2)}$$

where A_c and A_0 are the absorbances of DNA in the presence [0.050 mg/mL] and absence of NPs. A_{obs} signifies the change in absorbance on varying the concentration of MoO_3 NPs between 0.005 mg/mL and 0.050 mg/mL.

The binding ability was further monitored by fluorescence measurements. 6 mg of DNA was added to ethidium bromide solution (6 mg in 0.1 M tris-HCl at pH 7.2) and the fluorescence was monitored. On addition of MoO_3 NPs (0.025 mg/mL to 0.450 mg/mL), the fluorescence intensities were measured at an excitation wavelength of 515 nm [15]. The efficiency of fluorescence quenching was measured using Stern Volmer equation (3), where K_{SV} is the Stern-Volmer constant, [Q] represents the concentration of MoO_3 NPs, F_0 and F indicate fluorescence intensities in the absence and presence of nanoparticles [12].

$$\frac{F_0}{F} = 1 + K_{SV} \text{ ------ Eq.(3)}$$

The intrinsic binding constant, K_b indicating the interaction between MoO_3 NPs and ct-DNA was evaluated using equation (4).

$$log\frac{F_0-F}{F} = log\ K_b + n\ log\ [Q] \quad \text{------ Eq.(4)}$$

where [Q] represents the concentration of MoO_3 NPs, which acts as the quencher, K_b and n indicate the binding constant and number of binding sites in base pairs, respectively.

2.6. Cytotoxicity studies

A549 (human lung cancer) cells seeded onto 96-well plates (20,000 cells per well) were cultured for 24 hours at 37 °C and 5% CO_2 in an incubator. A 0.2 µm syringe filter was used to filter out 10 mg/mL of MoO_3 NPs NPs in DMEM medium. Using untreated wells as a control, the wells containing grown cells were further diluted with DMEM media to reach final concentrations of 25, 50, 100, 150, and 200 µg/mL. The studies were conducted in triplicate, and average values were noted. The plates were incubated for an additional 24 h following the addition of MoO_3 NPs, and the medium from the wells were discarded after aspiration. After adding 100 µL of a 0.5 mg/mL MTT solution in phosphate buffer and incubating for two hours, formazan crystals formed. The supernatant was removed from each well and 100 µL of DMSO was added. The absorbance at 570 nm was measured using a microplate reader. A-549 cells were used as blank with three wells per plate and the degree of cell viability was evaluated using equation (5).

$$Percentage\ of\ cell\ viability = \frac{Average\ absorbance\ of\ treated}{Average\ absorbance\ of\ control} \times 100\text{------}$$

Eq.(5)

3. Results and Discussion

3.1. Characterization of MoO_3 NPs

UV-Visible spectrum of *Cardiospermum halicacabum* leaf extract (Fig.1a) displays λ_{max} at 263 and 330 nm owing to π→π* transitions in the aromatic rings of flavonoids and phenolic compounds [13]. UV–visible DRS of green synthesized MoO_3 NPs is presented in Fig. 1b. The absorption spectrum of MoO_3 NPs shows a strong band at 353 nm indicating $O^{2-}\rightarrow Mo^{6+}$ transition of electrons from valence band to conduction band resulting in electronic excitation [16]. The band gap of MoO_3 NPs derived from *Cardiospermum halicacabum* was evaluated using Kubelka–Munk equation Equation (6).

$$(\alpha h\nu)^2 = kE_g - h\nu\text{------- Eq.(6)}$$

where *a*, k, and Eg represent absorption coefficient, Boltzmann constant, separation between valence and conduction bands respectively. Tauc's plot of $(ahv)^2$ as a function of *hv* is presented in Fig.1c from which the band gap is estimated by extrapolation toward the energy axis. The evaluated band gap of 2.48 eV correlates with the values reported in literature for MoO_3 NPs [16]. The fluorescence spectrum of MoO_3 NPs was recorded by varying the excitation wavelength from 210 to 350 nm (Fig.2). Maximum fluorescence intensity was observed at 210 nm, which was optimised for further studies. Excitation dependent emission is exhibited owing to surface defect states resulting in generation of miscellaneous emission sites. Molybdenum oxide exhibits luminescence peaks due to the radiative decay of self-trapped excitons. The traps are associated with certain intrinsic defects such as oxygen vacancies, or even more complex clusters of oxygen vacancies, which affects the molybdenum ion valence related to the charge transfer from O vacancies to Mo. The peak at 466 and 544 nm could be associated with the Mo^{6+} d–d band transition [17].

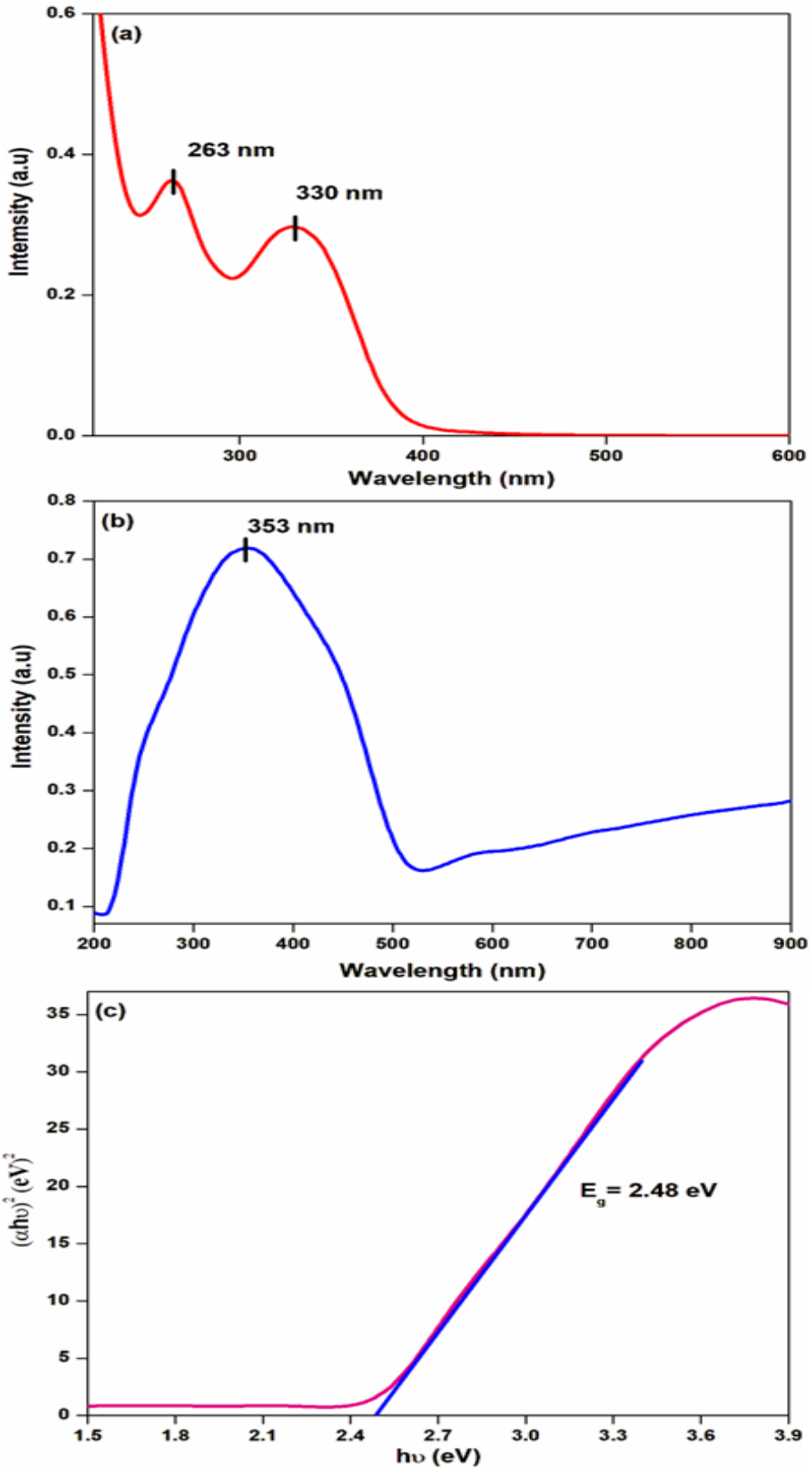

Fig. 1. (a) UV-Visible spectra of *Cardiospermum halicacabum* leaf extract, (b) UV-Vis DRS of MoO_3 NPs and (c) Tauc's plot of $(ahv)^2$ as a function of *hv*

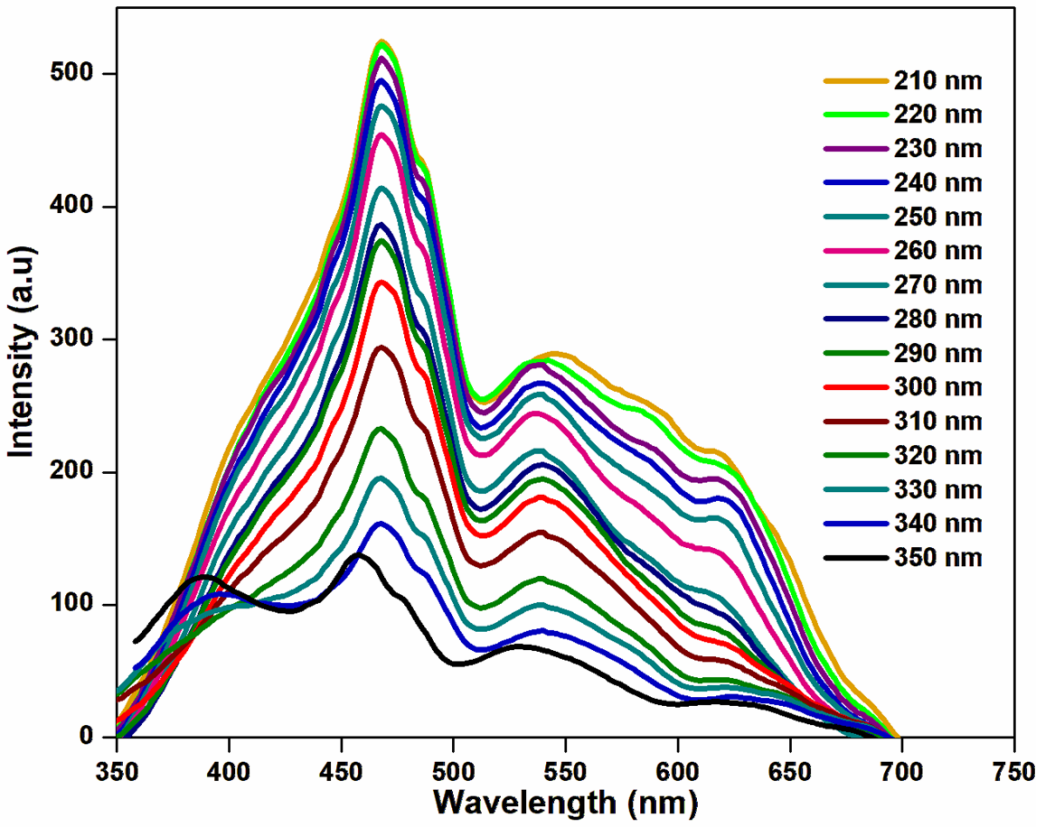

Fig. 2. Photoluminescence spectra of MoO_3 NPs [λ_{ex} = 210 to 350 nm]

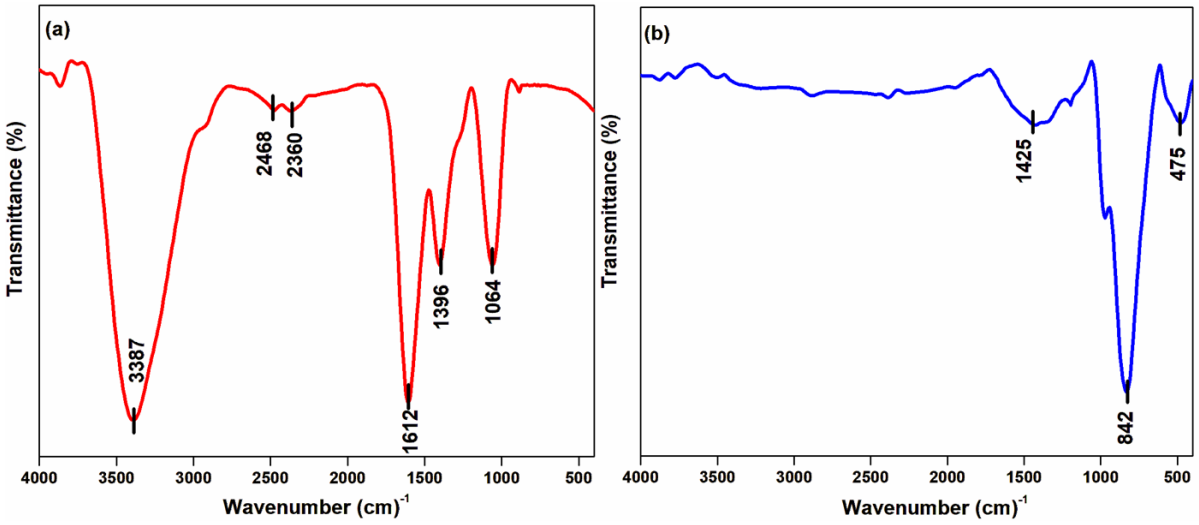

Fig. 3. FT-IR Spectra of (a) *Cardiospermum halicacabum* leaf extract and (b) MoO_3 NPs

FT-IR studies were performed with *Cardiospermum halicacabum* leaf extract and the synthesised MoO_3 NPs to identify the functional groups involved in the formation and stabilisation of NPs [Fig. 3]. The band observed at 3387 cm^{-1} in *Cardiospermum halicacabum* leaf extract [Fig. 3a] confirms the -OH group of phenols. The peak at 1612 cm^{-1} corresponds to carbonyl stretching. The peak at 1396 cm^{-1} due to N-H stretching of aromatic amine. C-O stretching corresponding to ether linkages (flavonoids) is observed at 1064 cm^{-1} [18]. In the FT-IR spectrum of MoO_3 NPs [Fig. 3b], the peak corresponding to N-H stretching of aromatic amine in the plant extract at 1396 cm^{-1} is shifted to 1425 cm^{-1} due to the interaction of biomolecules with the nanoparticles. Additionally, the signals located at 842 cm^{-1} and 475 cm^{-1} are associated to Mo-O-Mo stretching [19].

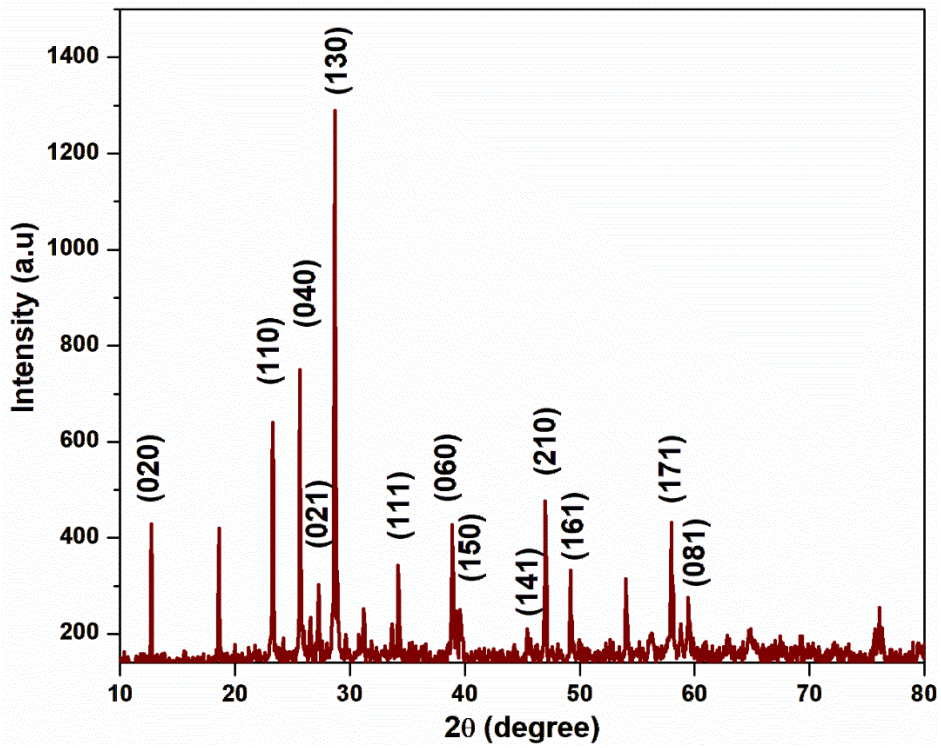

Fig. 4. X-Ray Diffraction pattern of MoO_3 NPs

Using X-Ray Diffraction analysis, the crystallinity and phase morphology of the synthesised MoO_3 NPs were assessed, and the pattern is shown in Fig. 4. The presence of (020), (110), (040), (021), (130), (111), (060), (150), (141), (210), (161), (171) and (081) crystal planes is confirmed by the diffraction peaks emerging at diffraction angles 12.72, 22.96, 25.68, 27.10, 28.51, 34.31, 39.01, 39.46, 45.48, 47.88, 49.10, 57.93 and 59.44. Diffraction peaks fit well with that of MoO_3 (JCPDS Card No.-05- 0508 [3]. By applying Debye-Scherrer's equation Eq.(7), the crystallite size is determined to be 69 nm.

$d = k\lambda/(\beta cos\theta)$ ------- Eq.(7)

where d, k, λ, ß and θ represent crystal size, Scherrer's constant, wavelength of X-rays, full width at half maximum and Bragg's angle respectively.

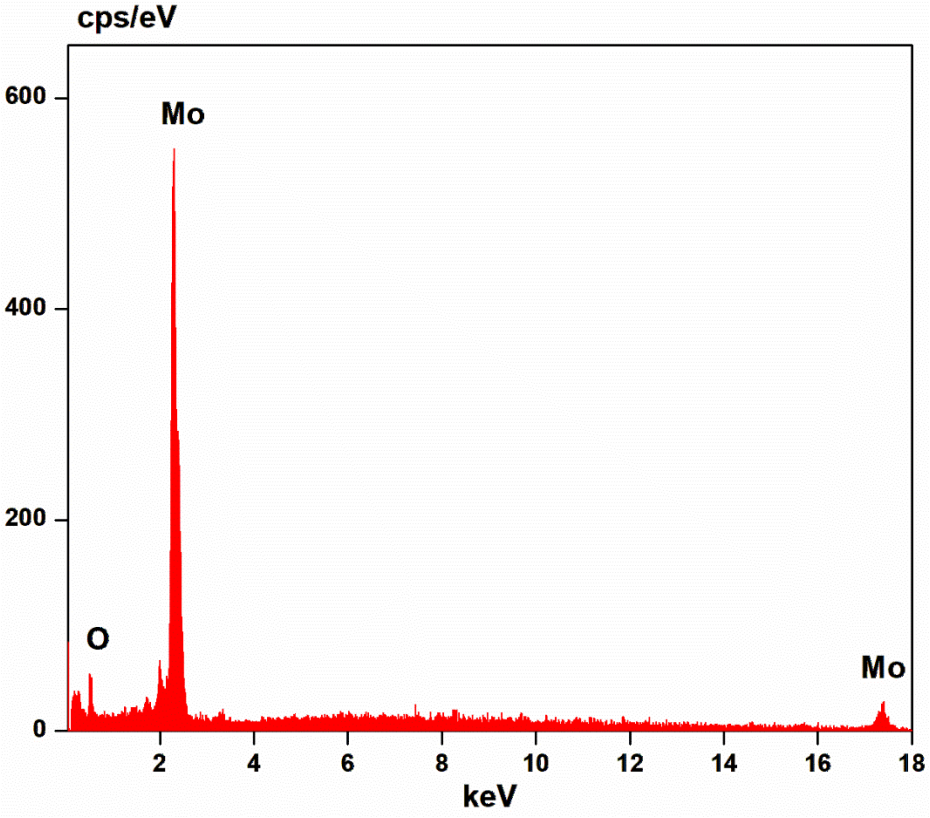

Fig. 5. Energy-Dispersive X-Ray pattern of MoO_3 NPs

The EDX pattern of MoO_3 NPs derived from *Cardiospermum halicacabum* leaf extract is presented in Fig.5, which confirms the presence of molybdenum (21.44%) and oxygen (78.56%). This further confirms the purity of the prepared nanoparticles.

XPS survey spectrum (Fig. 6a) is utilized to estimate the binding energies of molybdenum and oxygen. 3d core-level spectrum of Mo (Fig. 6b) shows peaks corresponding to binding energies of 232.4 and 235.6 eV, which correspond to Mo 3d spin-orbit splitting, Mo $3d_{5/2}$ and Mo $3d_{3/2}$. which is associated with the fully oxidised state of Mo (Mo^{6+}) as reported in literature. Figure 6(c) depicts the O 1s core level XPS spectrum which shows a binding energy of 530.3 eV, corresponding to lattice oxide (O^{2-}) sites. Thus, it is evident that the MoO_3 NPs comprises of Mo^{6+} and O^{2-} sites and is free from impurities [19].

TEM images of the MoO_3 NPs presented in Fig.7a show the presence of spherical particles with agglomeration. The particle size (Fig.7b) is predominantly distributed between 25 to 65 nm, and the average particle size is 45 nm.

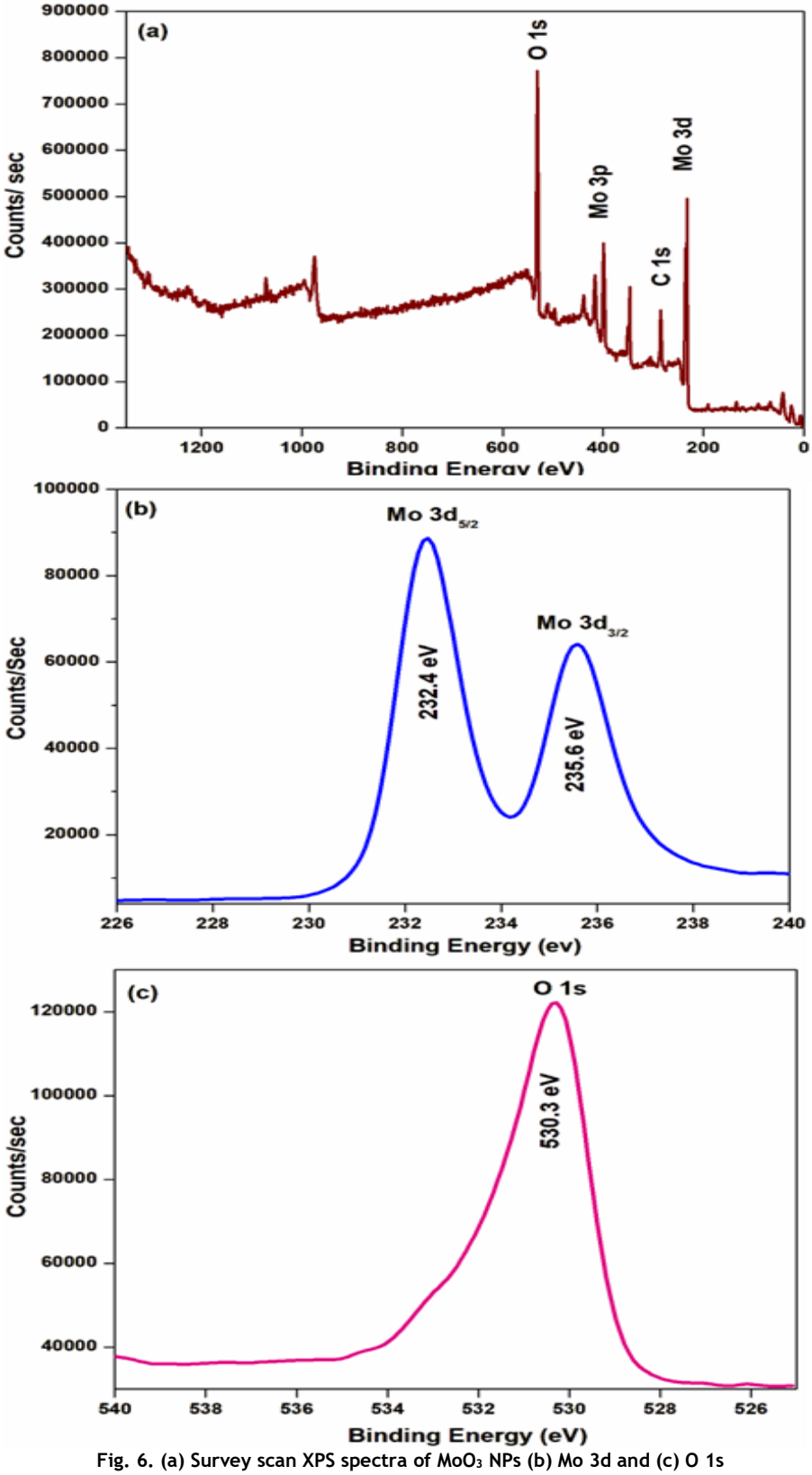

Fig. 6. (a) Survey scan XPS spectra of MoO_3 NPs (b) Mo 3d and (c) O 1s

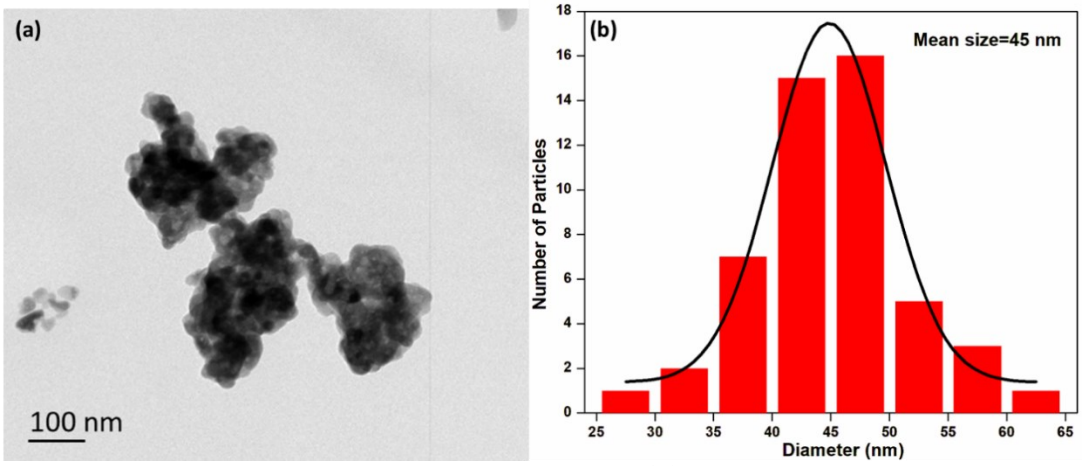

Fig. 7 (a) HRTEM image of MoO_3 NPs and (b) SAED Pattern

3.2. Fluorescence sensing of Pb^{2+} ions

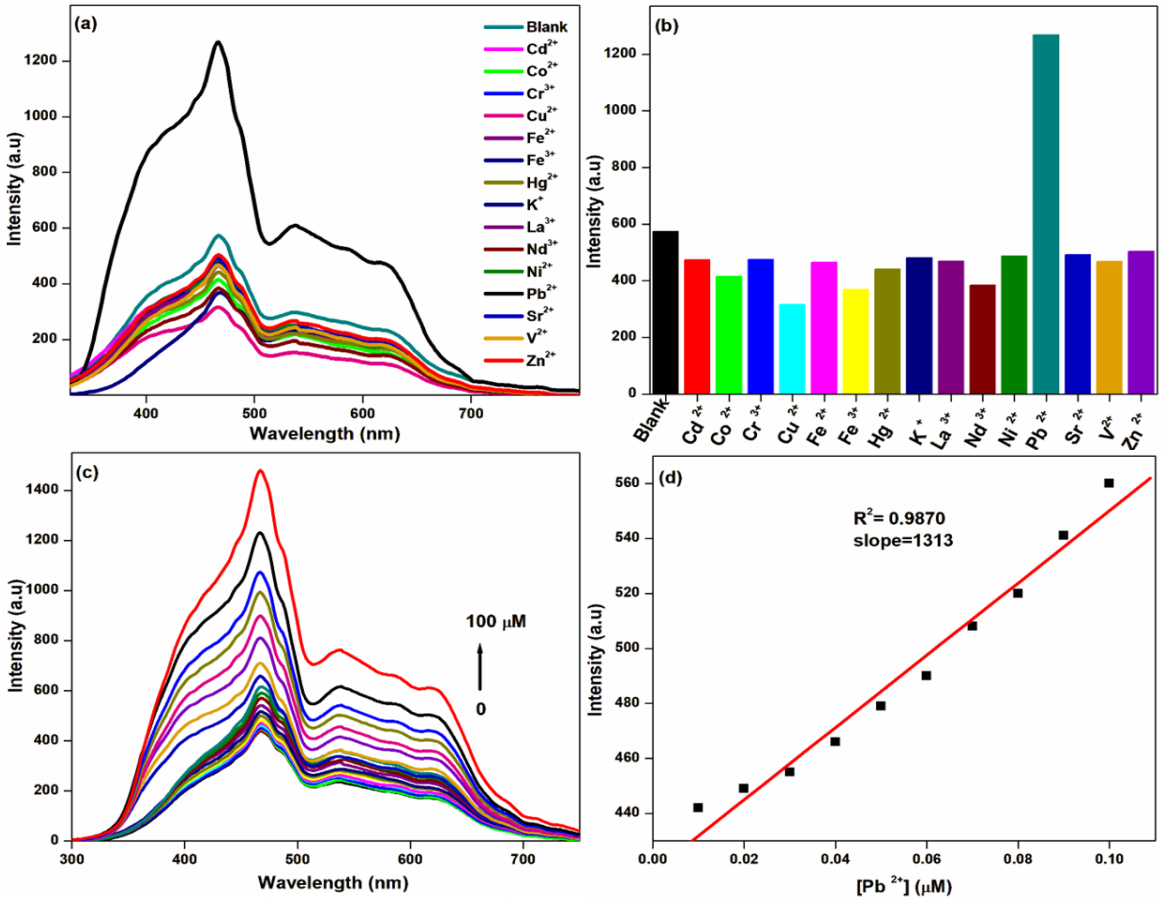

Fig. 8. (a) PL Spectra for fluorescence sensing of different metal ions with MoO_3 NPs, (b) Bar plot of emission intensity of MoO_3 NPs vs different metal ions (c) Fluorescence spectra of MoO_3 NPs with Pb^{2+} in the concentration range 0.01-100 μM, (d) Linear plot of fluorescence intensity vs $[Pb]^{2+}$ (0.01-0.1μM)

Selectivity studies play a prominent role in determining the metal ions suitable for study. In order to evaluate the sensitivity of MoO_3 NPs towards different metal ions, their fluorescence response towards various metal ions, viz., Cd^{2+}, Zn^{2+}, V^{2+}, Nd^{3+}, Fe^{2+}, Fe^{3+}, Cu^{2+}, Sr^{2+}, La^{3+}, Pb^{2+}, Ni^{2+}, Co^{2+}, $Cr^{3+}$and Hg^{2+}ions were measured. Fig.8a,b shows the fluorescence spectra of MoO_3 NPs upon the addition of 100 μM various metal ions, among which Pb^{2+} shows maximum fluorescence enhancement.

For further studies, the concentration of MoO_3 NPs was maintained constant, and the concentration of Pb^{2+} was varied between 0.01 and 100 μM. The fluorescence response on varying the concentration of metal ions was monitored and the results are displayed in Fig.8c. A linear correlation between concentration and fluorescence intensity is observed with a correlation coefficient of 0.9870. Limit of detection for fluorescence sensing of Pb^{2+} is calculated with the aid of the calibration curve (Fig.8d) of fluorescence intensity against concentration of Pb^{2+} ions and standard deviation of the blank using Eq.1. The limit of detection is calculated as 4.13×10^{-8} M.

Enhancement in fluorescence is observed on addition of Pb^{2+} ions with MoO_3 NPs. This is due to ionic-electrostatic interactions of organic capping agents present on the surface of MoO_3 NPs [20,21].

3.3. Binding studies with ct-DNA

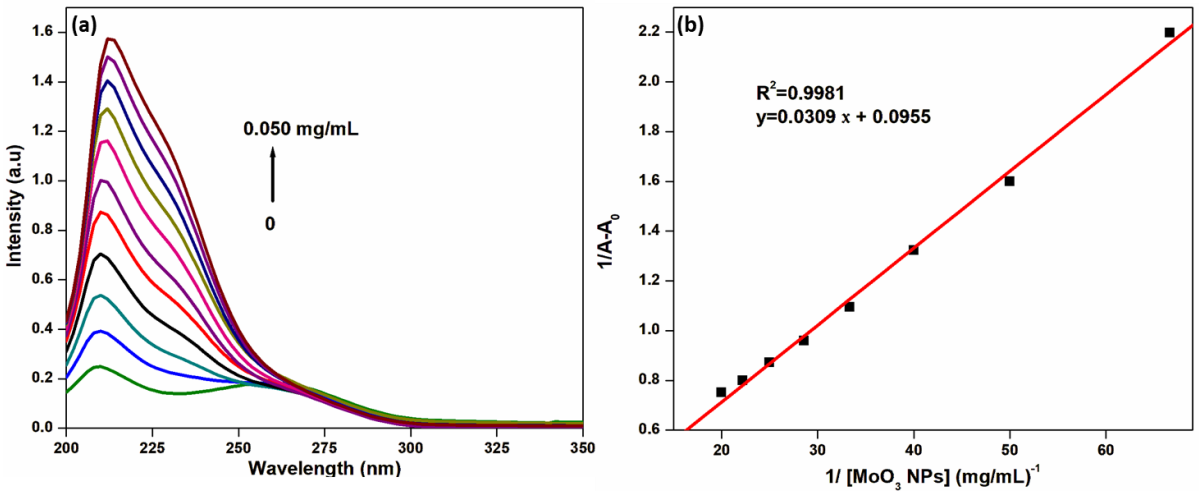

Fig. 9. (a) UV Vis Spectra of ct-DNA [100 µL] with MoO_3 NPs [0.005 mg/mL to 0.050 mg/mL] and (b) Benesi-Hildebrand plot

UV-Visible and fluorescence spectral techniques were employed to explore the nature of binding between MoO_3 NPs and ct-DNA. UV-Visible spectral studies recorded for ct-DNA (100 µL) with varying concentrations of nanoparticles are presented in fig.9a. The hyperchromic effect pronounced is attributed to the intercalation of nanoparticles with DNA. Benesi-Hildebrand plot displayed in Fig. 9b shows a linear relationship between the reciprocal concentration of MoO_3 NPs with $1/(A_{obs} - A_0)$. The plot shows the affinity of MoO_3 NPs for DNA, showing a K_{app} value (Eq. (2).) of 3.09 $(mg/mL)^{-1}$

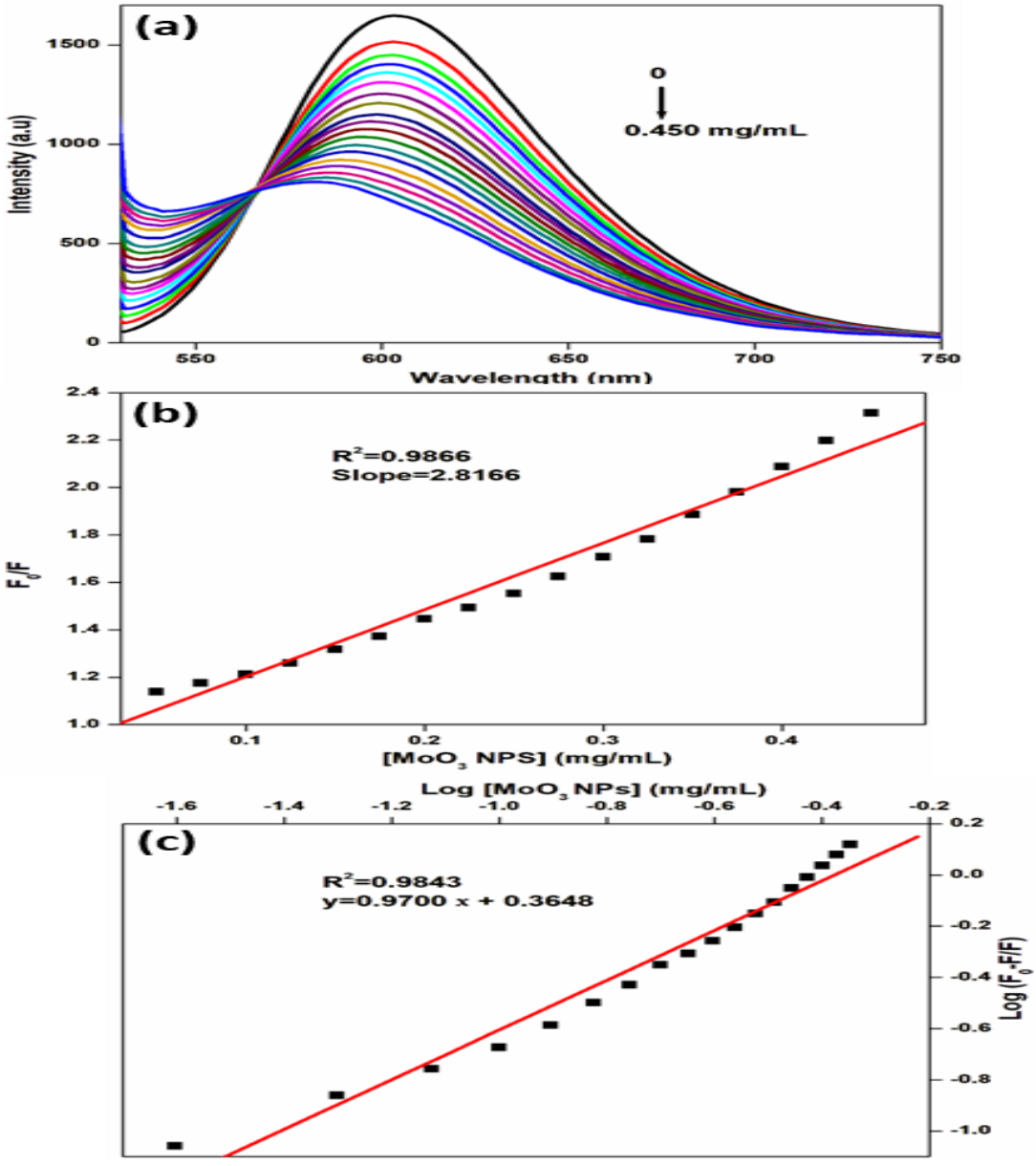

Fig. 10. (a) Photoluminescence spectra of EB-DNA with MoO_3 NPs [0 to 0.450 mg/mL), (b) Stern-Volmer plot of F_0/F vs. [MoO_3 NPs] and (c) Scatchard plot of log [(F_0-F)/F] vs. log [MoO_3 NPs]

Competitive binding of MoO_3 NPs with ct-DNA was studied with Ethidium Bromide (EB) fluorescence quenching assay. EB is a DNA binding fluorophore which can measure the extent of binding between NPs and DNA with different concentrations of MoO_3 NPs. The emission spectra of EB intercalated with ct-DNA with increasing concentrations of nanoparticles is presented in fig. 10a. The fluorescence intensity of MoO_3 NPs drops due to its intercalation with ct-DNA, which alters the surface defects [15]. The quenching pattern was further analysed using Stern-Volmer equation by monitoring fluorescence at 609 nm. The slope of the plot of F_0/F versus [MoO_3 NPs] (Fig.10b) was used to calculate the Stern-Volmer constant as 2.82 mg/mL (R^2=0.9866) based on Eq. (3), further supporting strong intercalation between MoO_3 NPs and DNA [14]. Fig. 10c showing a plot of log(F_0/F)/F vs log [MoO_3 NPs] and Eq. (4) were used to determine the number of binding sites and binding constant to be 0.97 and 2.32 $(mg/mL)^{-1}$.

3.4. Cytotoxicity of MoO_3 NPs against A-549 cell line

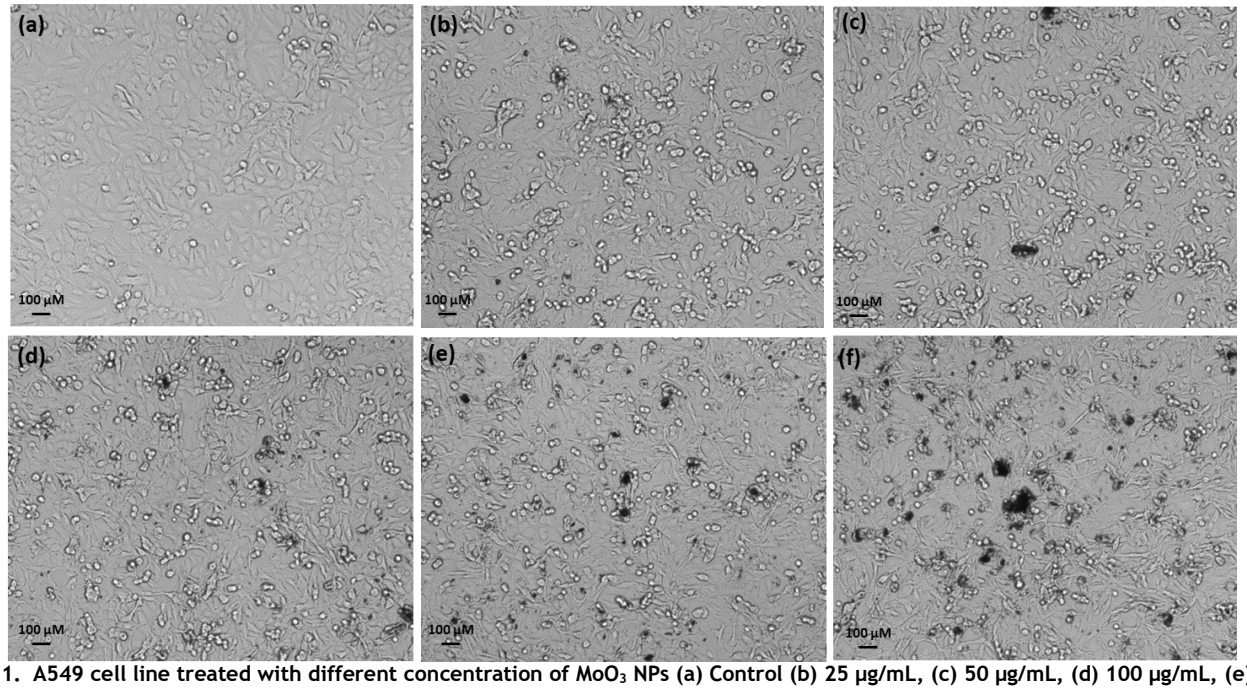

Fig. 11. A549 cell line treated with different concentration of MoO_3 NPs (a) Control (b) 25 µg/mL, (c) 50 µg/mL, (d) 100 µg/mL, (e) 150 µg/mL, (f) 200 µg/mL

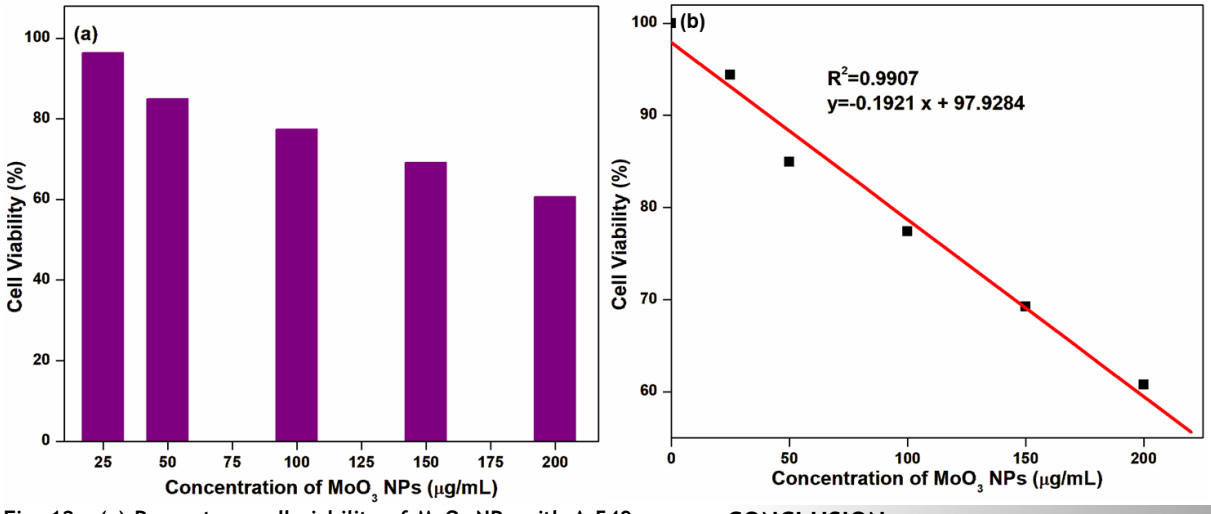

Fig. 12. (a) Percentage cell viability of MoO_3 NPs with A-549 Cell line as a function of concentration [25 to 200µg/mL] (b) Linear plot of Cell viability vs. concentration of MoO_3 NPs

The cytotoxicity potential of MoO_3 NPs against A-549 human lung cancer cells was evaluated by varying the concentration of MoO_3 NPs (Fig.11a-f) between 25 and 200 µg/mL maintaining an incubation period of 24 h. An increase in concentration of nanoparticles contributes to a decrease in cell viability as exhibited in fig.12a. A plot of percentage of cell viability against the concentration of MoO_3 NPs shows linearity (Fig.12b) which is used to calculate the half maximal inhibitory concentration (IC_{50} value) of MoO_3 NPs as 249.5 µg/mL.

CONCLUSION

This study proposes green and cost-effective technique for synthesising molybdenum oxide nanoparticles using *Cardiospermum halicacabum* leaf extract. The functional groups contributing to the formation and stabilisation of nanoparticles were identified using FT-IR studies. The particle size was estimated as 69 nm and 45 nm using X-Ray Diffraction studies TEM analysis respectively. XPS data revealed that the surface of the nanoparticles is dominant with Mo^{6+} and O^{2-} sites and are free from impurities.

Limit of detection for fluorescent sensing of Pb^{2+} was determined as $4.13x10^{-8}$ M. Intercalative mode of binding of ct-DNA with MoO_3 NPs was evaluated by UV-Visible and Fluorescence Spectra. Cell

viability studies and IC_{50} value suggested their potential against A549 cell lines. Thus, the synthesised nanoparticles find environmental, catalytic and biological applications.

REFERENCES

- S. Rajeswari, S. Thavamani, and T. Peter, "Solanum torvum Derived Zirconium Oxide Nanoparticles as Fluorescent Sensors and Photocatalysts," *Chem. Sel.* 10. 2025, 1–10, e01000. http://doi.org/10.1002/slct.202501000.
- R. Muthukumar Sivaraman, K. D. J. Gracia, S. S. Thavamani, T. P. Amaladhas, S. Devanesan, M. S. AlSalhi, N. N. Asemi, S. Natarajan, "CeO_2-$CePO_4$ and Ag@CeO_2-$CePO_4$ nanocomposites from *Penaeus semisulcatus* for heavy metals sensing, UV shielding and cytotoxic applications," *Arab. J. Chem.* 17 (2024) e105382. http://doi.org/10.1016/j.arabjc.2023.105382.
- K. S. Shruthi, N. Chandrasekhar, B. S. Surendra, M. Mahadeva Swamy and N. S. Basavaraju, " Fabrication of cost-effective green assisted synthesis of MoO_3 NPs: its photocatalytic activity and electrochemical sensing actions on lead, mercury, and paracetamol molecules," *Sens. Technol.*, 2, 2024, http://doi.org/10.1080/28361466.2024.2316612.
- R. M. Sivaraman, K. D. J. Gracia, S. S. Thavamani, T. P. Amaladhas, S. Devanesan, M. S. AlSalhi, "Green synthesis of La_2O_3–$LaPO_4$ nanocomposites using *Charybdis natator* for DNA binding, cytotoxic, catalytic, and luminescence applications," *Green Process. Synth.*13 (2024) e20240092. http://doi.org/10.1515/gps-2024-0092.
- T. A. Devi, R. M. Sivaraman, S. S. Thavamani, T. P. Amaladhas, M. S. AlSalhi, S. Devanesan, M. M. Kannan, "Green synthesis of plasmonic nanoparticles using *Sargassum ilicifolium* and application in photocatalytic degradation of cationic dyes," *Environ. Res.* 208 (2022) e112642. http://doi.org/10.1016/j.envres.2021.112642.
- S. Kaur, N. Arora, and S. Kaur, "Characterization of Yellow Pigments Produced by Pencillium sp. under Solid State Cultivation," *J. Biotechnol. Biomater.*, 07, 2017, 2-4. http://doi.org/10.4172/2155-952x.1000259.
- J. Liu, Q. Zhang, Xue, H. Zhang,Y. Bai, L.Wu, Z. Zhai, G.Jin "Fluorescence characteristics of aqueous synthesized tin oxide quantum dots for the detection of heavy metal ions in contaminated water," *Nanomaterials*, 9, 2019. http://doi.org/10.3390/nano9091294.
- M. S. Collin, S. K. Venkatraman, N. Vijayakumar, V. Kanimozhi, S. M. Arbaaz, R. G. Sibiya Stacey, J. Anusha, R. Choudhary, V. Lvov, G.I Tovar, F. Senatov, S. Koppala, S. Swamiappan "Bioaccumulation of lead (Pb) and its effects on human: A review," *J. Hazard. Mater. Adv.*, 7, 2022, 0-7. http://doi.org/10.1016/j.hazadv.2022.100094.
- K. D. J. Gracia, S. S. Thavamani, T. P. Amaladhas, S. Devanesan, M. Ahmed, M.M. Kannan, "Valorisation of bio-derived fluorescent carbon dots for metal sensing, DNA binding and bioimaging," *Chemosphere.* 298 (2022) e134128. http://doi.org/10.1016/j.chemosphere.2022.134128.
- K. D. J. Gracia, R. M. Sivaraman, S. S. Thavamani, T. P. Amaladhas, S. Devanesan, M. S. AlSalhi, M. Balakrishnan, "Nitrogen doped fluorescent carbon dots from Delonix regia for Fe(III) and cysteine sensing, DNA binding and bioimaging," *Arab. J. Chem.* 16 (2023) e105109. http://doi.org/10.1016/j.arabjc.2023.105109.
- M. Khorasani-Motlagh, M. Noroozifar, A. Moodi, and S. Niroomand, "Fluorescence studies, DNA binding properties and antimicrobial activity of a dysprosium(III) complex containing 1,10-phenanthroline," *J. Photochem. Photobiol. B Biol.*, 127, 2013, 192–201. http://doi.org/10.1016/j.jphotobiol.2013.08.009.
- S. U. Rehman, T. Sarwar, M. A. Husain, H. M. Ishqi, and M. Tabish, "Studying non-covalent drug-DNA interactions," *Arch. Biochem. Biophys.*, 576, 2015, 49–60. http://doi.org/10.1016/j.abb.2015.03.024.
- A. P. Suresh, N. Paramakrishnan, M. Basavaraju, and K. Mruthunjaya, "A Comprehensive Review on Cardiospermum halicacabum," *J. Nat. Remedies*, 23, 2023, 283–293, http://doi.org/10.18311/jnr/2023/29382.
- K. D. J. Gracia, R. M. Sivaraman, S. S. Thavamani, T. P. Amaladhas, "Bio-Derived Fluorescent Carbon Dots for Metal Sensing and DNA Binding Applications," *Chem. sel.* 8 (2023) e202204583. http://doi.org/10.1002/slct.202204583.
- S. Patel, P. Patel, S. B. Undre, S. R. Pandya, M. Singh, and S. Bakshi, "DNA binding and dispersion activities of titanium dioxide nanoparticles with UV / vis spectrophotometry, fluorescence spectroscopy and physicochemical analysis at physiological temperature," *J. Mol. Liq.*, 213, 2016, 304–311. http://doi.org/10.1016/j.molliq.2015.11.002.
- B. Gowtham, V. Ponnuswamy, G. Pradeesh, J. Chandrasekaran, and D. Aradhana, "MoO_3 overview: hexagonal plate-like MoO_3 nanoparticles prepared by precipitation method," *J. Mater. Sci. Mater. Electron.*, 29, 2018, 6835–6843. http://doi.org/10.1007/s10854-018-8670-7.
- O. Kamoun, A. Mami, M. A. Amara, R. Vidu, and M. Amlouk, "Nanostructured Fe, Co-codoped MoO3 thin films," *Micromachines*, 10, 2019. http://doi.org/10.3390/mi10020138.
- T. R and L. M, "Comparative Studies of Phytochemical and Antioxidant Activity of in Vivo Plant and in Vitro Callus Extract of Cardiospermum Halicacabum L.," *Asian J. Pharm. Clin. Res.*, 14, 2021, 94–103. http://doi.org/10.22159/ajpcr.2021.v14i8.42197.
- G.P. Nunna, H. K. Siddarapu, V. J. Nimmagadda, M. H. Obili, T.J. Ko, J. Lim, and J. Choi "Biogenic Synthesis of High-Performance *α*-MoO_3 Nanoparticles from Tryptophan Derivatives for Antimicrobial Agents and Electrode Materials of Supercapacitors," Int. J. *Energy Res.*, 2023, e6715319, http://doi.org/10.1155/2023/6715319.
- F. Ahmed, H. Kabir, and H. Xiong, "Dual Colorimetric Sensor for Hg^{2+} /Pb^{2+} and an Efficient Catalyst Based on Silver Nanoparticles Mediating by the Root Extract of Bistorta amplexicaulis," *Front. Chem.*, 8, 2020, 1–15. http://doi.org/10.3389/fchem.2020.591958.
- M. L. Desai, H. Basu, S. Saha, R. K. Singhal, and S. K. Kailasa, "One pot synthesis of fluorescent gold nanoclusters from Curcuma longa extract for independent detection of Cd^{2+}, Zn^{2+} and Cu^{2+} ions with high sensitivity," *J. Mol. Liq.*, 304, 2020, e112697. http://doi.org/10.1016/j.molliq.2020.112697.